NANO LETTERS
Letter
Cite This: Nano Lett. 2018, 18, 6981−6988
pubs.acs.org/NanoLett

In Vivo Laser-Mediated Retinal Ganglion Cell Optoporation Using $K_V1.1$ Conjugated Gold Nanoparticles

Ariel M. Wilson,[†,§] Javier Mazzaferri,[‡] Éric Bergeron,[§] Sergiy Patskovsky,[§] Paule Marcoux-Valiquette,[§] Santiago Costantino,[*,‡] Przemyslaw Sapieha,[*,†,‡] and Michel Meunier[*,§]

[†]Department of Biochemistry, Maisonneuve-Rosemont Research Center and [‡]Department of Ophthalmology, Maisonneuve-Rosemont Research Center, University of Montreal, Montreal, Quebec, Canada, H1T 2M4

[§]Department of Engineering Physics, Polytechnique Montréal, Montreal, Quebec, Canada, H3C 3A7

Supporting Information

ABSTRACT: Vision loss caused by retinal diseases affects hundreds of millions of individuals worldwide. The retina is a delicate central nervous system tissue stratified into layers of cells with distinct roles. Currently, there is a void in treatments that selectively target diseased retinal cells, and current therapeutic paradigms present complications associated with off-target effects. Herein, as a proof of concept, we introduce an in vivo method using a femtosecond laser to locally optoporate retinal ganglion cells (RGCs) targeted with functionalized gold nanoparticles (AuNPs). We provide evidence that AuNPs functionalized with an antibody toward the cell-surface voltage-gated K^+ channel subunit $K_V1.1$ can selectively deliver fluorescently tagged siRNAs or fluorescein isothiocyanate-dextran dye into retinal cells when irradiated with an 800 nm 100 fs laser. Importantly, neither AuNP administration nor irradiation resulted in RGC death. This system provides a novel, non-viral-based approach that has the potential to selectively target retinal cells in diseased regions while sparing healthy areas and may be harnessed in future cell-specific therapies for retinal degenerative diseases.

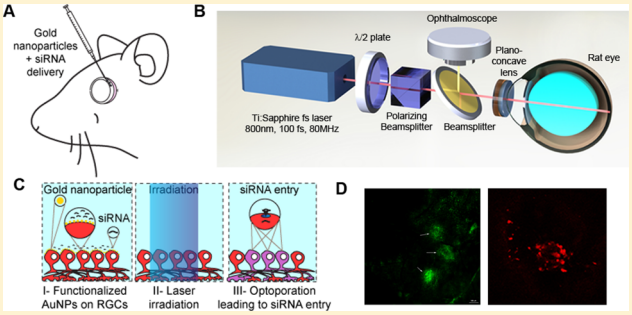

KEYWORDS: *Retinal cell optoporation, femtosecond laser, in vivo irradiation, bioconjugated gold nanoparticles*

Of all sensorial impairments, the loss of sight is the most feared.[1] Retinal degenerative diseases such as adult-onset glaucoma affect large portions of the population: over 50 million people worldwide, with 47 million having loss of sight in both eyes. As the diagnostic tools improve, the number of cases is expected to rise, and a recent study predicts that there will be 76 million people with glaucoma in 2020.[2] Glaucoma causes vision loss secondary to the degeneration of a neuronal cell population called retinal ganglions cells (RGCs), although the exact causes of this loss are largely ill-defined. This and other debilitating retinal diseases currently have no cure, and treatments only slow disease progression, leading to modest visual improvement.

There is a need in retinal pharmacology for selective cell targeting to provide effective remedies. Significant advances have been made in gene therapy, and the success of Spark's FDA approval is auspicious for cell-specific retinal therapies.[3] Although the field of viral-based gene therapies have shown great promise,[4,5] disadvantages include limits in delivered transgene size and lack of specificity for diseased cells.[6] Other means of administration and treatment modalities require perpetual intravitreal administrations and can lead to undesired side-effects including neuronal toxicity.[7,8] Hence, the lack of targeted, localized, and nontoxic delivery mechanisms undermines the full potential of therapies to treat retinal diseases.

Given that the structures leading to the retina are translucent and the light path is unobstructed, we devised a laser-based optoporation method to target retinal cells. The method presented herein is based on ultrafast femtosecond (fs, 10^{-15} s) laser irradiation at 800 nm of antibody (Ab)-functionalized gold nanoparticles (AuNPs), leading to transient cell membrane opening (optoporation) and the incorporation of exogenous molecules into targeted cells.[9−13] It uses spherical AuNPs to provide a unique double selectivity: Ab-AuNPs target cell-specific surface markers, and a high-precision laser beam ensures delivery exclusively to localized areas of the retina, thus avoiding off-target side effects. The mechanism is based on the plasmonic phenomenon of AuNPs: upon the off-resonance irradiation, the highly localized electric field results in the formation of a nanoscale plasma leading to an increase in local temperature and creation of a nanobubble around the AuNP.[14−17] When this occurs to AuNPs in the proximity of a cell membrane, the dissipated energy creates nanopores in the lipid layer. Thus, substances such as exogenous DNA, small interfering RNA (siRNA), or cell-impermeable dyes may

Received: July 16, 2018
Revised: September 27, 2018
Published: October 4, 2018

DOI: 10.1021/acs.nanolett.8b02896
Nano Lett. 2018, 18, 6981−6988

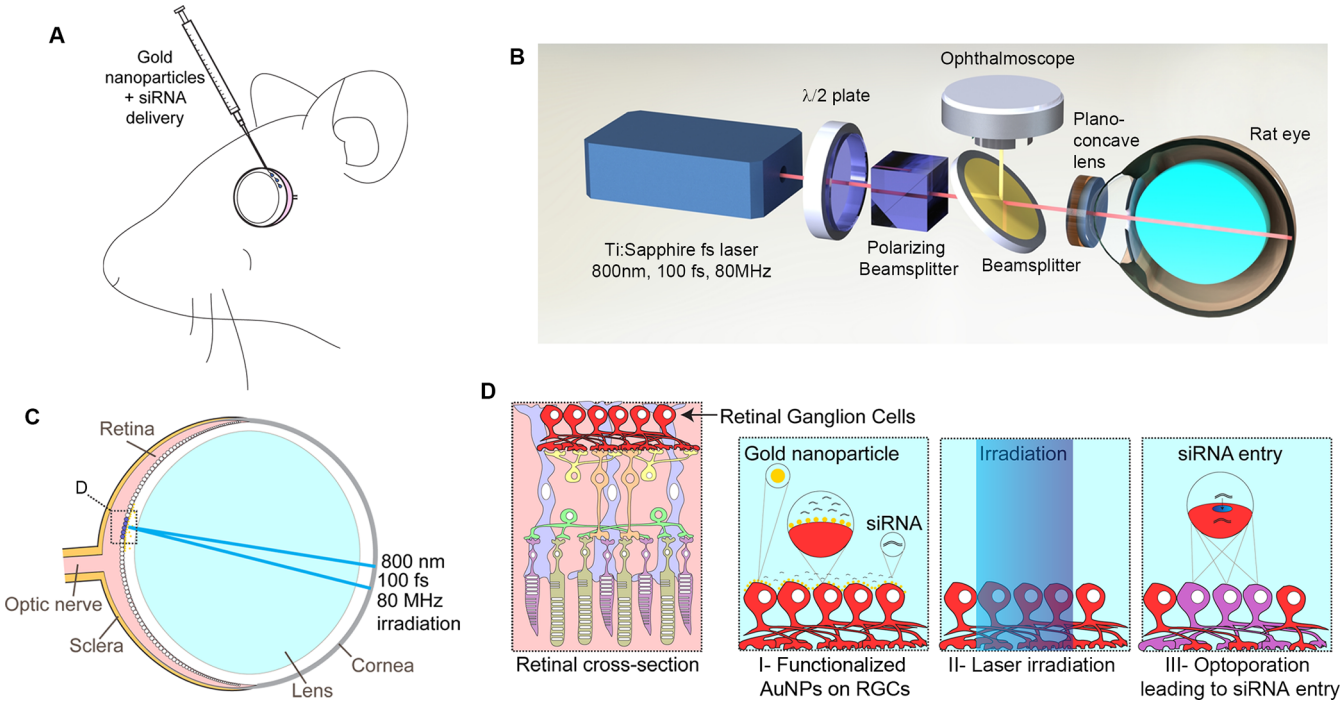

Figure 1. Design of optic system conducive to in vivo retinal cell optoporation. (A) Schematic of intravitreal injection of AuNPs, FITC, or siRNA into rat eyes. (B) Schematic of optical system designed to perform laser-mediated optoporation of rat retinal cells. The rat eye was positioned onto a plano-concave lens in the beam path of an ultrafast laser, and its fundus was visualized by ophthalmoscope. (C) Schematic of the laser-beam path converging onto retinal cells in the rat eye. (D) Schematic of targeted rat retinal cell optoporation by the femtosecond laser irradiation of RGCs. These steps are (I) functionalized AuNPs on RGCs, (II) laser irradiation, and (III) optoporation leading to siRNA entry.

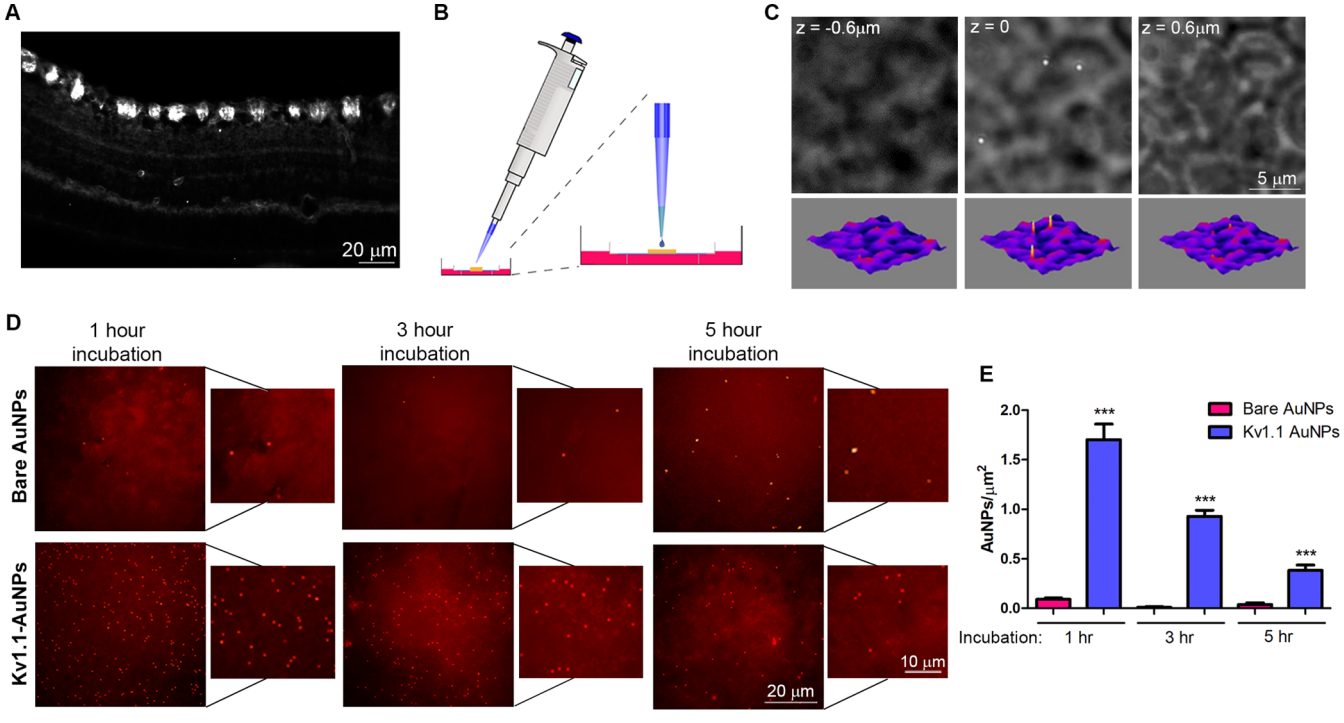

Figure 2. $K_V1.1$ AuNPs remain on the retinal surface longer than bare AuNPs. (A) $K_V1.1$ Ab immunohistochemistry on rat retinal cryosection. (B) Schematic of AuNP application on retinal explants. (C) Detection of $K_V1.1$ AuNPs on the retinal surface by dynamic 3D NP scanning. (D) Visualization of bare AuNPs and $K_V1.1$ AuNPs on retinal explants by enhanced dark-field microscopy following 1, 3, and 5 h incubations. (E) Quantification of bare AuNPs and $K_V1.1$ AuNPs detected on the surface of retinal explants. Data are means plus or minus the standard error of the mean, analyzed by a Student unpaired *t*-test (triple asterisks indicate $P < 0.001$).

penetrate into the cell by diffusion through the nanopore. Due to the fluidity of the lipid layer and because the irradiation is localized on a nanoscale, the membrane recovers without affecting the viability of the irradiated cell. Because biological

DOI: 10.1021/acs.nanolett.8b02896
Nano Lett. 2018, 18, 6981−6988

tissues absorb energy very weakly at 800 nm and AuNPs minimize heat absorption in the near-infrared, no further cellular damage is caused.[14,18]

We previously demonstrated that femtosecond laser irradiation of 100 nm AuNPs can optoporate human cancer cells in vitro.[9] Furthermore, we confirmed the precision of our technique by selectively optoporating one cell type in a co-culture setting using Ab-coupled AuNPs.[10] We further demonstrated selective cell labeling and detection by reflected light microscopy and immunofluorescence of Au nanorods functionalized with cell-surface voltage-gated K^+ channel subunit $K_V1.1$ Abs ($K_V1.1$ AuNRs).[19] Additionally, we have shown that plasmonic AuNPs can be engineered to optimize the efficiency of the technique.[20,21] Here, we demonstrate in vivo optoporation by locally delivering cell-impermeable dyes or siRNA into ultrafast laser-irradiated RGCs targeted with Ab-AuNPs. We provide evidence for successful in vivo optoporation of rat retinal cells with 100 fs laser pulses (with powers from 120 to 700 mW at the cornea) in the presence of $K_V1.1$ AuNPs targeting RGCs with fluorescein isothiocyanate (FITC)-dextran (2 MDa) or Cy3-siRNA. Furthermore, we confirmed that neither irradiation nor AuNP administration resulted in RGC death. This targeted laser-irradiation-based approach has the potential to locally deliver siRNA or small biomolecules to retinal cells in specific zones of the eye requiring treatment without adversely impacting surrounding healthy tissue.

Results. *Design of Optical System for in Vivo Retinal Cell Optoporation.* Successful in vivo laser-mediated optoporation requires contact between AuNP and the surface of irradiated cells. We opted for intravitreal injections because this administration route offers the highest bioavailability of AuNPs to retinal cells due to the proximity of the vitreous humor to cells on the retinal surface (Figure 1A).[22] We concomitantly injected a cell-impermeable FITC-dextran dye or fluorescently tagged siRNA to assess cellular intake of macromolecules subsequent to irradiation. Following AuNP and FITC-dextran/siRNA administration and incubation, we placed a plano-concave lens in contact with the eye, adding a hydrogel layer on the corneal surface of the anesthetised rat (Figure 1B). This lens and variable-length optical relay minimized focusing and optical aberrations of the cornea−air interface. This optical system allowed us to couple the femtosecond laser beam with that of a confocal ophthalmoscope for the visualization of the rat fundus to control the position and focus to irradiate the appropriate layer of retinal cells (Figure 1B). We illuminated a focused beam on the rat retina to optoporate locally (Figure 1C). The optoporation method is also selective with cell-specificity obtained with AuNPs targeting RGCs. This AuNP selectivity is achieved by the process of bioconjugation, by which a stable covalent link is made between AuNPs and Abs. The described system is designed to deliver femtosecond laser irradiation to RGCs in the presence of bioconjugated AuNPs to induce the uptake of siRNA or FITC-dextran (Figure 1D).

Selection of $K_V1.1$ Antibody to Target RGCs. $K_V1.1$ was selected to target RGCs based on the fact that targeted cell optoporation with antibody-coupled nanoparticles requires a cell-specific antigen on the cell surface (Figure 2A). There are numerous well-characterized cell-specific antigens used to label RGCs, such as the Brn3 family members Brn3a−c, RBPMS, βIII-tubulin, and Thy.1.[23−28] However, they could not be used in our study for the following reasons: Brn3a−c are intracellular transcription factors,[29] RBPMS is a cytoplasmic protein,[27] and βIII-tubulin is a microtubule element,[30] none of which are expressed at the cell surface. Thy1 (CD90) is a cell-surface glycoprotein, but its axonal localization[31] renders it nonspecific because RGC axons project radially from the cell body across the retinal surface to converge at the center of the retina. By irradiating nanoparticles conjugated to antibodies binding to both cell somas and axons, it would be impossible to optoporate one local area without targeting axons projecting to RGC cell bodies located distally in the retina (Figure S1). There are no known surface-expressed soma antigens specific to RGCs; therefore, we opted for $K_V1.1$, an RGC enriched channel protein. $K_V1.1$ is predominantly expressed by RGCs,[32] and we have previously characterized the coupling of $K_V1.1$ to NPs.[33]

$K_V1.1$ AuNPs Retained on the Retinal Surface. To attain cell-specific optoporation and to reduce the overall power of the laser used, we functionalized AuNPs with an Ab targeting the RGC-enriched cell-surface voltage-gated K^+ channel subunit $K_V1.1$ (Figure 2A). To assess whether AuNP functionalization elongated the retention time of AuNPs on the retinal surface, we applied 5 μL of bare AuNPs or $K_V1.1$ AuNPs (50 μg/mL) on retinal explants and incubated them for 1, 3, and 5 h (Figure 2B). We next confirmed the cell-surface NP position on the retina given that the 10−20 μm thick inner limiting membrane (ILM) above the ganglion cell layer might prevent $K_V1.1$ AuNPs from reaching the cell surface because the efficacy of NP penetrance through the ILM varies.[34−36] We performed 3D imaging by using reflected light microscopy in which an immersion objective with a high numerical aperture provides a high 3D resolution, allowing the reliable detection and localization of plasmonic NPs on the cell membrane.[19,37] Figure 2C depicts representative images rendered by microscopy z-scan of the NPs−tissue complex. When a NP focal plane is coincident with tissue surface (0 μm z position), the 100 nm AuNP scattering intensity is highest. A slight deviation from the focal point results in the decreasing of the scattering intensity ($z = \pm 0.2$ μm) up to complete disappearance of the NPs signature ($z = \pm 0.6$ μm) (Figure S2). Corresponding dynamic 3D NPs scanning can be seen in the ESI video (Video S1). The video travels a total distance in z of 3.5 μm, and the circular patterns of cells that surround and emerge below the Kv1.1 AuNPs suggest they are not stuck on the ILM but have reached the cell surface. Because AuNP detection occurred within the first layer of retinal cells, we can conclude they are localized to the ganglion cell layer.

Following incubation with AuNPs, explants were fixed, rinsed, mounted, and imaged by enhanced dark-field microscopy (Figure 2D). Quantification of AuNPs revealed that $K_V1.1$ AuNPs significantly outnumbered bare AuNPs on the surface of retinal explants after 1, 3, and 5 h of incubation followed by serial washes (Figure 2E). These data demonstrate that the bioconjugation of AuNPs with $K_V1.1$ Abs successfully targets RGCs and, thus, significantly increases AuNP retention on the retinal surface, even after hours of incubation and rinsing when compared to bare AuNPs. This finding is advantageous in the context of in vivo intravitreal administration, as the back of the eye is filled with vitreous and aqueous humor that flows across the retinal surface and could affect AuNP−cell interactions.[38]

Laser Irradiation in the Presence of $K_V1.1$ AuNPs and Provocation of Optoporation of RGCs. Having demonstrated that $K_V1.1$ Ab-conjugated AuNPs remained on the retinal

DOI: 10.1021/acs.nanolett.8b02896
Nano Lett. 2018, 18, 6981−6988

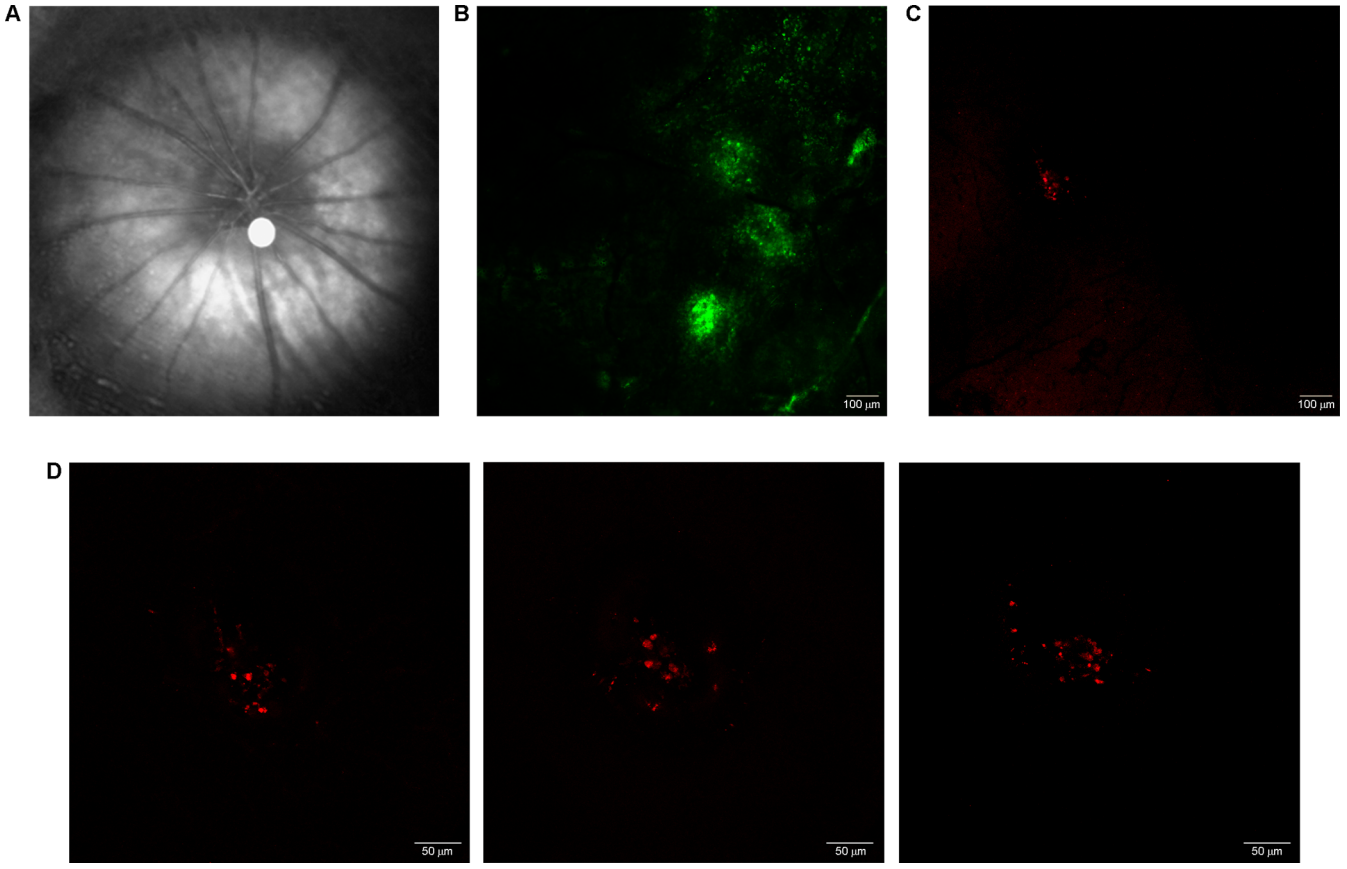

Figure 3. Laser irradiation in the presence of $K_V1.1$ AuNPs and yielding of optoporation of retinal cells. (A) Rat ocular fundus ophthalmoscope visualization through a plano-concave lens. (B) Confocal microscopy of in vivo optoporated rat retinal cells in the presence of $K_V1.1$ AuNPs, FITC-dextran (green, optoporation dye), and laser (100 fs pulses, 800 nm, 80 MHz) at 350 mW for 15 s. Scale bar: 100 μm (representative of n = 10). (C) Confocal microscopy of in vivo optoporated rat retinal cells in the presence of $K_V1.1$ AuNPs, Cy3-siRNA (red, fluorescently labeled siRNA), and laser (100 fs pulses, 800 nm, 80 MHz) at 350 mW for 15 s (scale bar of 100 μm) (representative of n = 10). (D) Confocal microscopy of in vivo optoporated rat retinal cells in the presence of $K_V1.1$ AuNPs, Cy3-siRNA, and laser at 120 mW (left panel), 350 mW (middle panel), and 700 mW (right panel) for 15 s (scale bar of 50 μm) (representative of n = 4).

surface (Figure 2C–E), we next administered $K_V1.1$ AuNPs intravitreally in anesthetized rats concomitantly to FITC-dextran and waited 3 h prior to irradiation to allow the $K_V1.1$ AuNPs to settle on the retinal surface onto RGCs. Anesthetized rats were placed on a warming blanket to prevent ketamine- and xylazine-induced cataract formation,[39,40] an opacification of the eye that would prevent the laser beam from reaching the retinal surface. Retinal fundus was visualized by ophthalmoscope (Figure 3A), and upon focusing on the retinal surface at a spot diameter estimated at 100 μm, fixed (nonscanned) laser irradiations were performed at powers of 120, 350, or 700 mW. The laser system successfully optoporated rat retinal cells with 100 fs laser pulses (power of 120, 350, and 700 mW, 15–30 s) in the presence of $K_V1.1$ AuNPs targeting RGCs and FITC-dextran (2 MDa) (n = 10, Figure 3B). We further tested the ability of our laser system to optoporate exogenous genetic material by investigating uptake of Cy3-tagged siRNA. Similarly to FITC-dextran, the laser system lead to Cy3-siRNA entry into retinal cells at all tested 120, 350, and 700 mW powers (n = 4, Figure 3). Cell optoporation with FITC-dextran (2 MDa) suggests that the described approach is successful at delivering biomolecules, while the delivery of Cy3-siRNA establishes a proof of concept for the delivery of exogenous genetic material to targeted retinal cells.

$K_V1.1$ AuNP with Laser Irradiation: No Induction of RGC Death. We next tested for cellular toxicity secondary to in vivo laser-mediated cell optoporation. We either irradiated retinas in vivo, as described above or delivered $K_V1.1$ AuNPs into the vitreous and assessed RGC survival (Figure 4A). We allowed for a 7 day lag period between injection of $K_V1.1$ AuNPs or irradiation and evaluation of RGC survival. This lag is sufficient to evaluate neural toxicity as RGC death by apoptosis or necrosis.[41–43] Retinal neurons are post-mitotic, and upon death by necrosis or apoptosis, their cell body is cleared from the retinal surface and, therefore, no longer detected by immunohistochemistry. Photomicrographs of RNA-binding protein RBPMS-labeled RGCs were taken of intact retinas as well as from saline-injected, bare-AuNP-injected, and $K_V1.1$-AuNP-injected eyes (Figure 4B). Quantifications revealed an absence of RGC death 1 week after administration, and RGC numbers were similar to control eyes (Figure 4C). Given that compounds injected into the vitreous have the capacity to reaching all areas of the retina, we quantified all regions of the retina. However, the optical system used for irradiation exclusively allows for the optoporation of central retinal areas visualized by ophthalmoscope, which, in the rat retina, corresponds to the central and medial portions of the retina (but not the most distal regions). Therefore, RGC quantification of irradiated retinas were carried out on

DOI: 10.1021/acs.nanolett.8b02896
Nano Lett. 2018, 18, 6981–6988

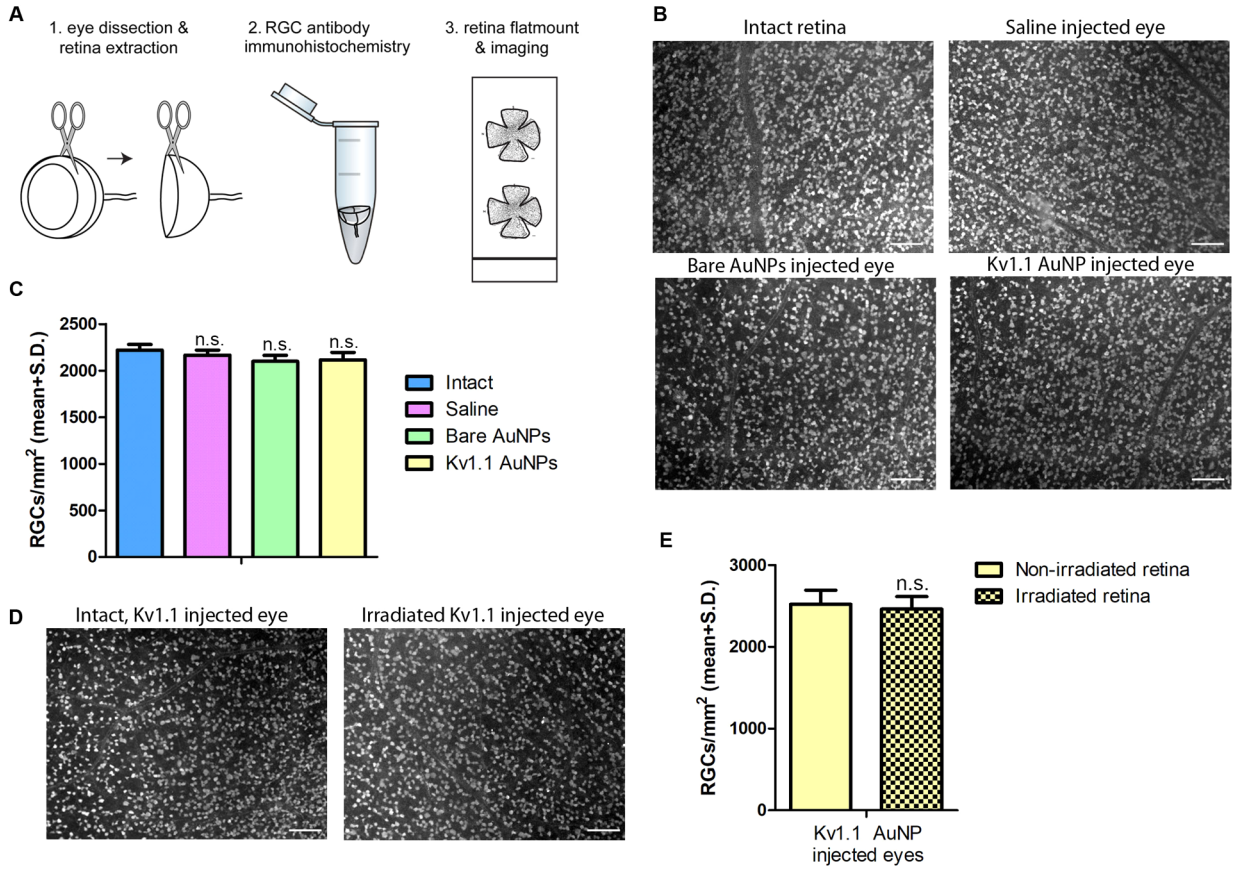

Figure 4. Laser irradiation with $K_V1.1$ AuNP and lack of RGC death. (A) Schematic of eye dissection, immunohistochemistry, and retinal flat mount for RGC quantification. (B) Photomicrographs of RBPMS-labeled RGCs of intact retina and 1 week after intravitreal injections of saline, bare AuNPs, and Kv1.1 AuNPs. (C) Quantification of RBPMS-positive RGCs 1 week after intravitreal injections of saline, bare AuNPs, and Kv1.1 AuNPs compared with intact retinas ($n = 6$). (D) Photomicrographs of RBPMS-labeled RGCs of Kv1.1 AuNP intravitreally injected retinas 1 week after injection (left) and irradiation (right). (E) Quantification of RBPMS-positive RGCs 1 week after intravitreal injections of Kv1.1 AuNPs with or without irradiation. ($n = 4$). Data are means plus or minus the standard error of the mean, analyzed by one-way ANOVA with a Bonferonni post-hoc test (panel C) or a Student unpaired *t*-test (panel E).

irradiated zones. Representative photomicrographs of irradiated and non-irradiated $K_V1.1$ AuNP RGCs are shown in Figure 4D. As discussed above, we did not detect RGC death in irradiated $K_V1.1$ AuNP injected eyes compared with non-irradiated controls (Figure 4E). Together, these data suggest that neither administration of $K_V1.1$ AuNP nor retinal cell irradiation is toxic for RGCs, and the overall approach proposed in this study may be of therapeutic utility.

Discussion. The current proof-of-principal study provides a novel method for in vivo targeted delivery of macromolecules into retinal cells. We demonstrate that femtosecond laser irradiation in the presence of conjugated AuNPs leads to localized in vivo optoporation of RGCs and cell-specific delivery of macromolecules. The double specificity of functionalized Ab-AuNPs targeting specific cell surface markers and fine-tuning of laser focalization on diseased cells represents a clear advantage over current, nonselective delivery approaches. This is of particular relevance in the treatment of retinal diseases because the retina is a post-mitotic tissue that does not readily regenerate. In this context, a therapeutic advantage will be attained with an approach that spares healthy retinal neurons.

The irradiation powers (up to 700 mW) and time of exposure (15−30 s) that rat retinas were exposed to in our study are elevated compared with those used in tissue culture but are required in dynamic irradiation conditions. Although the rat head is stabilized by a holder, the heartbeat moves the retinal surface during the irradiation process,[44] requiring extra power and time for optoporation. However, this increase did not result in RGC death. Furthermore, because the retina is a concave surface, the laser beam does not reach all retinal cell areas equally, which can result in certain retinal cells or retinal areas to be inadequately optoporated following illumination. Progressing to larger mammals such as rabbits or minipigs would improve the optics significantly and decrease the concavity of the surface within the 100 μm beam size range, thus increasing the likelihood of successful optoporation with lower powers. Initial reports of two-photon microscopy in the eye were also above the safety limits prescribed by the American National Standard for Safe Use of Lasers and have since been achieved within or below the safety limits.[45,46] Because our study consists of a proof-of-principle demonstration, we will build on these findings for the aim of achieving in vivo optoporation within the American National Standard for Safe Use of Lasers safety limits. Furthermore, testing in larger animals will be conducive to single-cell electroretinograms (ERGs), which is not feasible in rodent eyes, and thus determine how RGC function, and other cell types such as photoreceptors[47] are affected by femtosecond laser irradiation and optoporation.

DOI: 10.1021/acs.nanolett.8b02896
Nano Lett. 2018, 18, 6981−6988

This study opens novel therapeutic and research avenues by providing an integrated tool for the delivery of therapeutic biomolecules (genes, silencing RNAs, and drugs) to the back of the eye. siRNA molecules have the potential to treat blinding diseases by directly inhibiting local gene expression.[48] A benefit of siRNAs compared to Crisper-Cas9 is that they allow temporary gene product attenuation without gene ablation. This is particularly important when targets are critical to tissue homeostasis such as VEGF but is over-expressed in ocular pathologies such as age-related macular degeneration, diabetic retinopathy, and retinopathy of prematurity.[49−51] This method would allow for siRNA delivery, as well as that of other exogenous genetic material, to selective cell populations in targeted areas of the retina. In addition, given the extensive current use of laser technology in ophthalmic practice, our technology may be seamlessly inserted into current clinical setups.

Methodology. *Experimental Animals.* Animal procedures were performed in accordance with the guidelines of the Canadian Council on Animal Care for the use of experimental animals (www.ccac.ca). All surgeries were performed in adult, male Sprague Dawley rats (200−300 g, Charles River Canada).

Materials. $K_V1.1$ Ab (extracellular) (no. APC-161) was purchased from Alomone Laboratories (Jerusalem, Israel). OPSS-PEG(5 kDa)-NHS and HS-PEG (5 kDa) were purchased from Nanocs (New York, NY). Citrate-capped AuNPs were purchased from Nanopartz (50 μg/mL, 100 nm in diameter, A11−100, Loveland, CO) and stored at 4 °C in the dark to minimize photoinduced oxidation. Sterile sodium chloride solution (0.9%, saline) was purchased from Hospira (Saint-Laurent, Quebec, Canada). Tear Gel ophthalmic liquid gel was purchased from Alcon (Fort Worth, TX). Paraformaldehyde EM-grade solution (16%) and FluoroGel with Tris buffer mounting medium were purchased from Electron Microscopy Sciences (Hatfield, PA). FITC-dextran (2 MDa) and sucrose were purchased from Sigma (Saint Louis, MO). HBSS, Neurobasal A, Fungizone were purchased from Gibco (Thermofischer, Waltham, MA). Phosphate-buffered saline (PBS) was purchased from Wisent (Saint Bruno, Quebec). N2, B27, and L-glutamine were purchased from Invitrogen (Carlsbad, CA). Penicillin−streptomycin was purchased from Corning). Millicell 0.4 μm pore, 30 mm diameter cell culture inserts were purchased from EMD Millipore (Merck Millipore, Burlington, MA). Coverslips (22 mm × 50 mm), microscope slides (75 mm × 25 mm × 1 mm) and Tissue-Tek O.C.T compound were purchased from VWR (Radnor).

Nanoparticle Functionalization. AuNPs were functionalized by following a procedure reported previously.[10,33,52−54] Briefly, Ab bioconjugation to AuNPs was performed in sequential steps of Ab conjugation to OPSS-PEG-NHS followed by tethering of OPSS-PEG-Ab to AuNPs. To conjugate Abs to OPSS-PEG-NHS, $K_V1.1$ Abs were added to a solution of OPSS-PEG-NHS in Na_2CO_3 10 mM pH 8.5 (Ab/OPSS-PEG-NHS molar ratio of 1:1.88), resulting in a solution of OPSS-PEG-$K_V1.1$ solution. The OPSS-PEG-$K_V1.1$ solution was briefly vortexed and kept at 4 °C for 3 h. Tethering of OPSS-PEG-$K_V1.1$ to AuNPs was then performed using heterobifunctional PEG linkers by taking advantage of the strong covalent binding between sulfur and gold.[52] Citrate-coated AuNPs were treated with aqueous Na_2CO_3 (10 mM, pH 8.5) and a solution of OPSS-PEG-$K_V1.1$ and incubated for 1 h at 4 °C. An aqueous solution of 50 μM HS-PEG was added to the suspension of bioconjugated AuNPs to block the remaining free sites on the AuNP surface. After 1 h of incubation at 4 °C, the solution was centrifuged at 5000 rpm for 2 min,[55] and the supernatant was removed and replaced with saline for intravitreal administration.

Retinal Explants. Retinal explants were prepared as previously published.[56,57] Briefly, adult Sprague Dawley rat eyes were collected and the retinas dissected in dissection medium [HBSS solution containing penicillin−streptomycin (Sigma) and Fungizone (Gibco)]. Retina quadrants were placed retinal-ganglion side up onto cell-culture inserts (Millicell Cell Culture Inserts, 0.4 μm pore) in 6-well plates containing retinal explant culture medium [Neurobasal A medium (Invitrogen) supplemented with B27, N2 (Invitrogen), and penicillin−streptomycin]. Following 1 h of incubation in 37 °C 5% CO_2, 3 μL drops of AuNPs (bare or $K_V1.1$ AuNPs) were added to the surface of the retinal explants and incubated for 1, 3, or 5 h, rinsed in PBS, post-fixed in paraformaldehyde 4% at 4 °C overnight, further rinsed, mounted onto microscope slides with mounting medium and coverslips, and analyzed by modified dark-field microscopy.

Modified Dark-Field Microscopy. Precise NP imaging on retinal surfaces was performed with a previously published reflected light illumination setup[54] on an inverted Eclipse Ti microscope (Nikon) equipped with an 100× oil-immersion objective. This approach allows the detection of NPs attached to the nontransparent tissue sample with high contrast and spatial resolution.

Dynamic 3D NP Scanning. Samples were examined with immunoplasmonics microscopy as previously described by us on an inverted Eclipse Ti microscope (Nikon) equipped with a 100× oil-immersion objective.[33,54] Briefly, the microscopy image of a single plasmonic NP, which appears as an isolated bright dot, was aligned with the input slit on an imaging spectrograph equipped with a charge-coupled device detecting camera. A custom written LabView software performed 3D image acquisition.

AuNP Quantification. Manual quantification was performed to generate histograms from photomicrographs taken by enhanced dark-field microscopy. Identical 3 × 3 grids were placed on all images so as to separate every photomicrograph into 9 quadrants. All bright fluorescent spots in each quadrant were counted manually with ImageJ software to ensure all AuNPs were counted and that no duplicate counting occurred. When summed and averaged this revealed the number of nanoparticles per arbitrary unit. This count was subsequently converted to measurement units by adjusting to the photomicrograph scale. Details are shown in Figure S3.

Intravitreal Injections. Intravitreal injections have been previously described by our group.[58−61] Briefly, anesthetized rats with 2−3% isofluorane rats have 5 μL injected into the vitreous chamber using a Hamilton syringe adapted with a glass-pulled needle. For FITC-AuNP irradiation, $K_V1.1$ AuNPs were resuspended in 1% FITC diluted in 0.9% saline at a concentration of 100 μg/mL. For siRNA-AuNP irradiation, $K_V1.1$ AuNPs were resuspended in a 2 μg/mL siRNA solution diluted in 0.9% saline.

Optical System. The power of a 800 nm Ti:sapphire 100 fs, 80 MHz system is modulated using a half-wave-plate and a polarizing beam splitter. After going through the shutter (not shown), the laser beam divergence angle is fine-tuned with a 1:1 telescope consisting of two convergent lenses with equal focal distances (not shown). The purpose of the telescope is to minimize the size of the beam focal spot on the eye retina. To

DOI: 10.1021/acs.nanolett.8b02896
Nano Lett. 2018, 18, 6981−6988

reduce the aberrations of the first interface of the cornea, a plane-concave lens is placed in contact with the eye, and a 10× microscope objective (not shown) is used to compensate for the loss of refractive power. A Heidelberg Spectralis HRA ophthalmoscope for fundus visualization is used to monitor simultaneously the retina and the laser spot. Details are shown in Figure 1B.

Irradiation of the Rodent Eye. AuNPs-FITC were injected intravitreally 3 h prior to irradiation. Rats were anesthetized with a ketamize and xylazine mix (ketamine, 90 mg/kg; xylazine, 10 mg/kg). Corneas were covered with Tear-Gel ophthalmic hydrogel to prevent drying. Rats were placed onto a warm heating pad set at 37 °C to prevent anesthesia-induced hypothermia from opacifying the lens and cornea. Additional Tear-Gel was placed between the cornea and plano-concave lens through which the laser beam and ophthalmoscope were aligned. The eyes of anesthetized rats were placed in the beam path of the optical system, and several fixed irradiations were performed from 120 to 700 mW for 15−30 s. A spot size on the retina of approximately 100 μm was evaluated by the extent over which cells were fluorescent.

Histology. Eyes were removed subsequent to irradiation for the visualization of FITC or Cy3-siRNA signal visualization and 1 week following intravitreal injection, irradiation, or both for toxicity studies. Ocular globes were post-fixed in 4% paraformaldehyde, and either retinas were dissected as flatmounts and mounted onto microscope slides or subsequently incubated in 30% sucrose, embedded in optimal cutting temperature compound, and cryosectioned at 10 μm.

■ ASSOCIATED CONTENT

Supporting Information

The Supporting Information is available free of charge on the ACS Publications website at DOI: 10.1021/acs.nanolett.8b02896.

Figures showing the selection of Kv1.1 antibody to target RGCs, the AuNPs located on the retina, and a figure detailing the quantification of AuNPs on the retinal explants (PDF)

A video showing the dynamic 3D NPs scanning in support of Figure S2 (AVI)

■ AUTHOR INFORMATION

Corresponding Authors

*E-mail: santiago.costantino@umontreal.ca. Phone: 514-252-3400 ext 7711. Fax: 514-252-3430.

*E-mail: mike.sapieha@umontreal.ca. Phone: 514-252-3400 ext 7711. Fax: 514-252-3430.

*E-mail: michel.meunier@polymtl.ca. Phone: 514-340-4711 ext 4971. Fax: 514-340-5195.

ORCID

Michel Meunier: 0000-0002-2398-5602

Funding

This work was supported by the Consortium Québécois sur la Découverte du Médicament (CQDM), by NSERC (PRCS446655-13), and by CIHR (CPG 127773).

Notes

The authors declare the following competing financial interest(s): Polytechnique Montreal filed a provisional patent US (62/576,973) on October 25, 2017, entitled "Method and System for Delivering Exogenous Biomolecules into the Eye".

■ ACKNOWLEDGMENTS

A.M.W. held a fellowship from the Natural Sciences and Engineering Research Council of Canada (NSERC) (PDF-471745-2015). M.M. held a Canada Research Chair in laser technology for biomedical applications (950-208523) and is supported by NSERC (RGPIN-2013-9028). This work was supported by operating grants to P.S. from the Canadian Institutes of Health Research (353770), the Heart & Stroke Foundation Canada (G-16-00014658), The Foundation Fighting Blindness Canada, the Canadian Diabetes Association (OG-3-14-4544-PS), and Natural Sciences and Engineering Research Council of Canada (418637). P.S. holds the Wolfe Professorship in Translational Research and a Canada Research Chair in Retinal Cell Biology.

■ REFERENCES

(1) Scott, A.; Bressler, N.; Ffolkes, S.; Wittenborn, J.; Jorkasky, J. *JAMA ophthalmology* **2016**, *134* (10), 1111−1118.

(2) Tham, Y.-C.; Li, X.; Wong, T.; Quigley, H.; Aung, T.; Cheng, C.-Y. *Ophthalmology (Philadelphia)* **2014**, *121* (11), 2081−2090.

(3) *Medical Letter on Drugs & Therapeutics* **2018**, *60*, (1543), 53−55.

(4) Kampik, D.; Ali, R. R.; Larkin, D. F. P. *Exp. Eye Res.* **2012**, *95* (1), 54−9.

(5) Boye, S.; Lewin, A.; Hauswirth, W.; Boye, S. L. *Mol. Ther.* **2013**, *21* (3), 509−519.

(6) Liu, X.; Brandt, C.; Rasmussen, C.; Kaufman, P. *Can. J. Ophthalmol.* **2007**, *42* (3), 447−454.

(7) Wen, J.; Reina Torres, E.; Sherwood, J.; Challa, P.; Liu, K.; Li, G.; Chang, J. Y. H.; Cousins, S.; Schuman, S.; Mettu, P.; Stamer, W. D.; Overby, D.; Allingham, R. R. *Invest. Ophthalmol. Visual Sci.* **2017**, *58* (3), 1893−1898.

(8) Smith, S.; Smith, B.; Mohney, B. *Br. J. Ophthalmol.* **2014**, *98* (3), 292−297.

(9) Baumgart, J.; Humbert, L.; Boulais, É.; Lachaine, R.; Lebrun, J.-J.; Meunier, M. *Biomaterials* **2012**, *33* (7), 2345−50.

(10) Bergeron, E.; Boutopoulos, C.; Martel, R.; Torres, A.; Rodriguez, C.; Niskanen, J.; Lebrun, J.-J.; Winnik, F.; Sapieha, P.; Meunier, M. *Nanoscale* **2015**, *7* (42), 17836−47.

(11) Ding, W., Bergeron, E., Lachaine, R.; Meunier, M. Nanomaterial-assisted light- induced poration and transfection of mammalian cells. In *Applications of Nanoscience in Photomedicine*; Hamblin, M. R. a. A. P., Ed.; Woodhead Publishing: Sawston, UK, 2015; pp 331−376.

(12) Boulais, E.; Lachaine, R.; Hatef, A.; Meunier, M. *J. Photochem. Photobiol., C* **2013**, *17*, 26−49.

(13) Schomaker, M.; Heinemann, D.; Kalies, S.; Willenbrock, S.; Wagner, S.; Nolte, I.; Ripken, T.; Escobar, H. M.; Meyer, H.; Heisterkamp, A. *J. Nanobiotechnol.* **2015**, *13* (1), 10.

(14) Boulais, E.; Lachaine, R.; Meunier, M. *Nano Lett.* **2012**, *12* (9), 4763−4769.

(15) Dagallier, A.; Boulais, E.; Boutopoulos, C.; Lachaine, R.; Meunier, M. *Nanoscale* **2017**, *9* (9), 3023−3032.

(16) Boutopoulos, C.; Bergeron, E.; Meunier, M. *Journal of biophotonics* **2016**, *9* (1−2), 26−31.

(17) Boutopoulos, C.; Hatef, A.; Fortin Deschênes, M.; Meunier, M. *Nanoscale* **2015**, *7* (27), 11758−11765.

(18) Weissleder, R. *Nat. Biotechnol.* **2001**, *19* (4), 316−317.

(19) Bergeron, E.; Patskovsky, S.; Rioux, D.; Meunier, M. *Nanoscale* **2016**, *8* (27), 13263−13272.

(20) Lachaine, R.; Boulais, É.; Rioux, D.; Boutopoulos, C.; Meunier, M. *ACS Photonics* **2016**, *3* (11), 2158−2169.

(21) Lachaine, R.; Boutopoulos, C.; Lajoie, P.-Y.; Boulais, É.; Meunier, M. *Nano Lett.* **2016**, *16* (5), 3187−3194.

(22) Kompella, U.; Amrite, A.; Pacha Ravi, R.; Durazo, S. *Prog. Retinal Eye Res.* **2013**, *36*, 172−198.

(23) Nadal Nicolás, F.; Jiménez López, M.; Salinas Navarro, M.; Sobrado Calvo, P.; Alburquerque Béjar, J.; Vidal Sanz, M.; Agudo Barriuso, M. *PLoS One* **2012**, *7* (11), e49830−e49830.

DOI: 10.1021/acs.nanolett.8b02896
Nano Lett. 2018, 18, 6981−6988

(24) Nadal-Nicolas, F.; Jimenez-Lopez, M.; Sobrado Calvo, P.; Nieto-Lopez, L.; Canovas-Martinez, I.; Salinas Navarro, M.; Vidal Sanz, M.; Agudo, M. *Invest. Ophthalmol. Visual Sci.* **2009**, *50* (8), 3860−3868.
(25) Rodriguez, A.; de Sevilla Müller, L. P.; Brecha, N. *J. Comp. Neurol.* **2014**, *522* (6), 1411−1443.
(26) Barnstable, C. J.; Dräger, U. C. *Neuroscience* **1984**, *11* (4), 847−855.
(27) Kwong, J. M. K.; Caprioli, J.; Piri, N. *Invest. Ophthalmol. Visual Sci.* **2010**, *51* (2), 1052−1058.
(28) Sharma, R.; Netland, P. *Brain Res.* **2007**, *1176*, 11−17.
(29) He, X.; Treacy, M. N.; Simmons, D. M.; Ingraham, H. A.; Swanson, L. W.; Rosenfeld, M. G. *Nature* **1989**, *340* (6228), 35−41.
(30) Sullivan, K. F.; Cleveland, D. W. *Proc. Natl. Acad. Sci. U. S. A.* **1986**, *83* (12), 4327−4331.
(31) Barlow, J. Z.; Huntley, G. W. *J. Comp. Neurol.* **2000**, *421* (2), 215−233.
(32) Höltje, M.; Brunk, I.; Grosse, J.; Beyer, E.; Veh, R. W.; Bergmann, M.; Grosse, G.; Ahnert Hilger, G. *J. Neurosci. Res.* **2007**, *85* (1), 19−33.
(33) Bergeron, É.; Patskovsky, S.; Rioux, D.; Meunier, M. *Nanoscale* **2016**, *8* (27), 13263−13272.
(34) Gan, L.; Wang, J.; Zhao, Y.; Chen, D.; Zhu, C.; Liu, J.; Gan, Y. *Biomaterials* **2013**, *34* (24), 5978−5987.
(35) Kim, H.; Robinson, S.; Csaky, K. *Pharm. Res.* **2009**, *26* (2), 329−337.
(36) Koo, H.; Moon, H.; Han, H.; Na, J.; Huh, M.; Park, J.; Woo, S.; Park, K.; Kwon, I. C.; Kim, K.; Kim, H. *Biomaterials* **2012**, *33* (12), 3485−3493.
(37) Patskovsky, S.; Bergeron, E.; Rioux, D.; Meunier, M. *Journal of biophotonics* **2015**, *8* (5), 401−407.
(38) Goel, M.; Picciani, R.; Lee, R.; Bhattacharya, S. *Open Ophthalmol. J.* **2010**, *4*, 52−59.
(39) Livingston, A.; Low, J.; Morris, B. *Br. J. Pharmacol.* **1984**, *81* (1), 189−193.
(40) Calderone, L.; Grimes, P.; Shalev, M. *Exp. Eye Res.* **1986**, *42* (4), 331−337.
(41) Lebrun-Julien, F.; Bertrand, M.; De Backer, O.; Stellwagen, D.; Morales, C. R.; Di Polo, A.; Barker, P. A. *Proc. Natl. Acad. Sci. U. S. A.* **2010**, *107*, 3817−3822.
(42) Wilson, A.; Morquette, B.; Abdouh, M.; Unsain, N. s.; Barker, P.; Feinstein, E.; Bernier, G.; Di Polo, A. *J. Neurosci.* **2013**, *33* (5), 2205−2216.
(43) Bien, A.; Seidenbecher, C. I.; Bockers, T. M.; Sabel, B. A.; Kreutz, M. R. *J. Neurotrauma* **1999**, *16* (2), 153−163.
(44) de Kinkelder, R.; Kalkman, J.; Faber, D.; Schraa, O.; Kok, P. H. B.; Verbraak, F.; van Leeuwen, T. *Invest. Ophthalmol. Visual Sci.* **2011**, *52* (6), 3908−3913.
(45) Palczewska, G.; Stremplewski, P.; Suh, S.; Alexander, N.; Salom, D.; Dong, Z.; Ruminski, D.; Choi, E.; Sears, A.; Kern, T.; Wojtkowski, M.; Palczewski, K. *JCI insight* **2018**, *3* (17), 1 DOI: 10.1172/jci.insight.121555.
(46) Schwarz, C.; Sharma, R.; Fischer, W.; Chung, M.; Palczewska, G.; Palczewski, K.; Williams, D.; Hunter, J. *Biomed. Opt. Express* **2016**, *7* (12), 5148−5169.
(47) Palczewska, G.; Vinberg, F.; Stremplewski, P.; Bircher, M.; Salom, D.; Komar, K.; Zhang, J.; Cascella, M.; Wojtkowski, M.; Kefalov, V.; Palczewski, K. *Proc. Natl. Acad. Sci. U. S. A.* **2014**, *111* (50), E5445−E5454.
(48) Fire, A.; Xu, S.; Montgomery, M. K.; Kostas, S. A.; Driver, S. E.; Mello, C. C. *Nature* **1998**, *391* (6669), 806−811.
(49) Robinson, G. S.; Ju, M.; Shih, S. C.; Xu, X.; McMahon, G.; Caldwell, R. B.; Smith, L. E. *FASEB J.* **2001**, *15* (7), 1215−1217.
(50) Saint Geniez, M.; Maharaj, A. S. R.; Walshe, T.; Tucker, B.; Sekiyama, E.; Kurihara, T.; Darland, D.; Young, M.; D'Amore, P. *PLoS One* **2008**, *3* (11), e3554−e3554.
(51) Aiello, L. P.; Northrup, J. M.; Keyt, B. A.; Takagi, H.; Iwamoto, M. A. *Arch. Ophthalmol.* **1995**, *113* (12), 1538−1544.
(52) Hirsch, L. R., Halas, N. J., West, J. L. Whole-Blood Immunoassay Facilitated by Gold Nanoshell-Conjugate Antibodies. In *NanoBiotechnology Protocols*, Rosenthal, S. J., Wright, D. W., Ed.; Humana Press Inc.: Totowa, NJ, 2005; Vol. *303*, pp 101−111.
(53) Patskovsky, S.; Bergeron, E.; Meunier, M. *Journal of biophotonics* **2015**, *8* (1−2), 162−167.
(54) Patskovsky, S.; Bergeron, E.; Rioux, D.; Meunier, M. *Journal of biophotonics* **2015**, *8* (5), 401−407.
(55) Liu, T.; Thierry, B. *Langmuir* **2012**, *28* (44), 15634−15642.
(56) Bull, N.; Johnson, T.; Martin, K. *Protocol Exchange*, **2011** DOI: 10.1038/protex.2011.215.
(57) Bull, N.; Johnson, T.; Welsapar, G.; DeKorver, N.; Tomarev, S.; Martin, K. *Invest. Ophthalmol. Visual Sci.* **2011**, *52* (6), 3309−3320.
(58) Chen, J.; Connor, K.; Aderman, C.; Smith, L. E. H. *J. Clin. Invest.* **2008**, *118* (2), 526−33.
(59) Combadiere, C.; Feumi, C.; Raoul, W.; Keller, N.; Rodero, M.; Pezard, A.; Lavalette, S.; Houssier, M.; Jonet, L.; Picard, E.; Debre, P.; Sirinyan, M.; Deterre, P.; Ferroukhi, T.; Cohen, S. Y.; Chauvaud, D.; Jeanny, J. C.; Chemtob, S.; Behar-Cohen, F.; Sennlaub, F. *J. Clin. Invest.* **2007**, *117* (10), 2920−8.
(60) Pang, J.-J.; Chang, B.; Hawes, N.; Hurd, R.; Davisson, M.; Li, J.; Noorwez, S.; Malhotra, R.; McDowell, J. H.; Kaushal, S.; Hauswirth, W.; Nusinowitz, S.; Thompson, D.; Heckenlively, J. *Molecular vision* **2005**, *11*, 152−162.
(61) Sapieha, P. S.; Hauswirth, W. W.; Di Polo, A. *J. Neurosci. Res.* **2006**, *83* (6), 985−995.

DOI: 10.1021/acs.nanolett.8b02896
Nano Lett. 2018, 18, 6981−6988